IEICE TRANSACTIONS

on Fundamentals of Electronics, Communications and Computer Sciences

This advance publication article will be replaced by the finalized version after proofreading.

PSO-CGAN-based Iced Transmission Line Galloping Prediction Method

Yun LIANG[†a)], Degui YAO[†b)], Yang GAO[†c)], *and* Kaihua JIANG[††d)], *Nonmembers*

SUMMARY The phenomena of iced line galloping in overhead transmission lines, caused by wind or asymmetric icing, can directly result in structural damage, windage yaw discharge of conductor, and metal damage, posing significant risks to the operation of power systems. However, the existing prediction methods for iced line galloping are difficult to achieve accurate predictions due to the lack of a large amount of iced line galloping data that matches real-world conditions. To address these issues, this paper studies the overhead iced transmission line galloping response prediction. First, the models of finite element, aerodynamic coefficient, and aerodynamic excitation for the iced conductor are constructed. The dynamic response of the conductor is simulated using finite element software to obtain a dataset of conductor galloping under different parameters. Secondly, a particle swarm optimization-conditional generative adversarial network (PSO-CGAN) based iced transmission line galloping prediction model is proposed, where the weight parameters of loss function in CGAN are optimized by PSO. The model takes initial wind attack angle, wind speed, and span as inputs to output prediction results of iced transmission line galloping. Then, based on the dynamics and galloping features of the conductor, the effects of different initial wind attack angles, wind speeds, and icing thickness on galloping are analyzed. Finally, the superior performance of the proposed model is verified through simulations.

key words: *iced transmission line galloping prediction; finite element simulation; particle swarm optimization; conditional generative adversarial network*

1. Introduction

With the expansion of electricity demand and increasing requirements for secure power supply, the construction of power grids has accelerated, leading to the erection of transmission lines in complex and variable terrain and harsh weather conditions [1]. The transmission lines erected in natural environments is susceptible to extreme weather including icing and storms, resulting in successive overhead iced transmission line galloping faults in different regions [2]. Iced transmission line galloping faults refer to low-frequency, large-amplitude self-excited vibrations of transmission lines caused by wind and asymmetric icing, representing an aerodynamic instability phenomenon [3], [4]. Compared to ordinary transmission line galloping faults, iced transmission line galloping typically exhibits characteristics

of low frequency, large amplitude, and long duration due to the increase in conductor cross-sectional area and wind load caused by icing [5]. It can lead to faults such as windage yaw discharge, conductor erosion, phase-to-phase tripping, metal damage, and even conductor fracture and tower collapse in severe cases [6]–[9], posing significant hazards to the operation of power systems. Therefore, the study on iced transmission line galloping and its preventive measures holds essential theoretical and engineering value.

For iced transmission line galloping prediction, compared to field data collection experiments which are costly, time-consuming, challenging to control, and difficult to obtain results, efficient and low-cost methods such as finite element model simulation, wind tunnel test, and numerical simulation have been increasingly adopted by researchers for iced transmission line galloping prediction [10]. In [11], Zheng et al. presented a full multi-span two-degree-of-freedom iced covered transmission line model, established a nonlinear galloping model of multi-span conductors considering the influence of insulator strings, and derived its galloping equation. In [12], Huo et al. applied the Galerkin method to the continuous dynamic model to establish a mathematical model considering three torsional modes. Numerical procedures were implemented on the mathematical model to simulate the galloping feature, and an experiment was designed using a continuous model for conductor galloping to validate the aforementioned feature. In [13], Luo et al. designed a torsional tuned mass damper with eddy current mechanism to tackle the galloping problem of ultra-high-voltage transmission lines. For a full-span iced conductor with multiple torsional tuned mass dampers, motion equations of galloping were derived and discretized using the Galerkin method. In [14], Diana et al. simulated the system structure and predict iced line galloping based on finite element analysis, which is verified based on time domain simulations and energy methods, demonstrating good effectiveness from an engineering perspective. However, the existing traditional feature recognition-based and deterministic modeling-based iced line galloping methods have strong limitations. They cannot consider the randomness and uncertainty factors during the transmission line icing process, such as weather changes and wind speed fluctuations, and are difficult to handle the coupling effect of meteorological parameters, terrain features, and conductor structure characteristics, thus making them difficult to achieve accurate prediction of iced transmission line galloping.

Machine learning involves an algorithmic approach that

†The authors are with State Grid Henan Electric Power Company Electric Power Scientific Research Institute, Zhengzhou 450052, China
††The author is with State Grid Zhejiang Electric Power Company Electric Power Scientific Research Institute, Hangzhou 310014, China
a) E-mail: liangyun04@163.com
b) E-mail: 18840606681@126.com
c) E-mail: gaoyang198824@163.com
d) E-mail: jiangkaihua_cqu@163.com

autonomously examines data to determine underlying patterns and leverages these identified patterns to forecast outcomes for previously unseen data [15]. It proves to be efficient in tackling challenges characterized by intricate mechanisms and multiple influencing factors. In recent years, scholars have developed galloping prediction models based on machine learning methods. In [16], Wang et al. used support vector machine (SVM) classifier to predict meteorological conditions based on historical meteorological parameters. When the meteorological conditions meet the galloping criteria, they further considered the conductor parameters to implement galloping prediction by using the AdaBoost classifier. In [17], Yang et al. considered multiple environment factors and established a radial basis function (RBF) based galloping prediction model. They used galloping samples from Liaoning Province, China, from 2010 to 2015 as training and testing cases. In [18], Zhang et al. established a back propagation (BP) based transmission line galloping prediction model, which inputs environment factors and outputs transmission line galloping risk. However, existing traditional machine learning algorithms typically perform pattern recognition and prediction based on a large amount of existing data. For iced transmission line galloping prediction, acquiring a vast dataset with labels is a challenging task. The traditional machine learning algorithms lack the ability to generate new data based on existing real data, resulting in lower prediction accuracy. As a generative model, generative adversarial network (GAN) can learn the mathematical distribution of target data and perform a new similarity reconstruction to generate more random and diverse data samples. Due to its characteristics, GAN has been widely used in scenarios such as energy scenario reconstruction and smart power grid temporal data generation. In [19], Shi et al. presented a GAN-based image completion technology, where the constructed generator serves to replenish the absent image segments, while the discriminator assesses the effect of this completion and guides the generator learning to achieve good image completion results. In [20], Liang et al. employed a double adversarial training approach capable of precisely forecasting subsequent single or multiple frames of a video once the training is complete, demonstrating that GAN can be applied to various prediction fields. However, while the aforementioned studies have achieved certain advancements in galloping prediction of iced transmission lines, there are still the following issues.

- **Inadequate adaptability of iced conductor models:** Existing methods for constructing iced conductor models only consider partial influencing factors or assumptions, and cannot comprehensively consider the complexity and diversity of the conductor erection area [21]. Moreover, most existing methods for constructing iced conductor models are based on empirical or statistical approaches and lack rigorous physical foundations, which limits the generality and accuracy of the constructed iced conductor models, and makes them difficult to be extended to various scenarios.

- **Poor diversity of generated iced line galloping data samples due to neglecting scenario condition constraints:** Iced line galloping involves multiple factors such as wind speed, icing thickness, and galloping amplitude, and is often constrained by natural conditions such as weather and geography, making it difficult to obtain effective iced line galloping data. Traditional GANs ignore the scenario condition constraints when generating sample data, resulting in poor diversity of generated data samples and low fidelity to actual scenarios [22]. As a result, the training effectiveness and convergence speed of GAN are reduced, leading to low prediction accuracy.

- **Low iced line galloping prediction accuracy of traditional GAN due to fixed weight parameters:** GAN networks involve many weight parameters that need to be adjusted during the construction and training process, such as numerical deviation weight parameter and galloping morphology deviation weight parameter. Traditional methods mostly rely on experience to set weight parameters, and these weight parameters cannot be dynamically adjusted during the entire training process [23]. It easily leads to poor quality of generated data, excessive delay in network discrimination, and being trapped in local optima, resulting in significant reduction in the accuracy and stability of iced line galloping prediction.

This paper proposes a particle swarm optimization conditional generative adversarial network (PSO-CGAN) based iced transmission line galloping prediction model. Firstly, ansys parametric design language (APDL) is used to simulate the dynamic response of the LGJ-400/50 type conductor under different spans and initial wind attack angles by constructing a finite element model, obtaining a dataset of 2500 cases of conductor galloping responses with different parameters. Secondly, a multi-layer perceptron (MLP) is selected to form the CGAN model, which is trained based on the obtained dataset. The Wasserstein distance is utilized to quantify the disparity between the actual and the simulated distributions. The CGAN parameters are optimized based on the PSO algorithm to explore the appropriate weight parameters of numerical deviation and morphological deviation, improving the accuracy of iced line galloping prediction. Finally, the impact of initial wind attack angle, icing thickness, and wind speed on the galloping is examined. The effectiveness of the proposed model is verified through simulations.

The primary contributions are summarized below.

- **Construction of accurate finite element model for iced conductor:** An APDL approach is utilized to construct a finite element model. Fluent software is utilized to simulate the dynamic response under different conditions, including icing thickness, wind speed, galloping status, galloping amplitude, initial wind attack angle, and torsion angle. This model allows for accurate determination of conductor galloping responses, supporting

high-precision prediction of iced line galloping.

- **The iced line conductor galloping prediction based on improved CGAN:** Based on traditional GAN, an MLP is selected to form the discriminator and generator of CGAN, and the WasserStein distance is used to measure the disparity between the actual and simulated distributions, addressing the gradient explosion or vanishing during CGAN network training and improving the accuracy of iced line galloping prediction.

- **PSO-based CGAN parameter optimization:** A PSO-based CGAN parameter optimization method is proposed, which utilizes the PSO algorithm to explore appropriate weight parameters of numerical deviation and morphological deviation in the CGAN network. It reduces the discrimination delay of the network, improves the reliability of the discrimination results, and thereby enhances the accuracy and stability of iced line galloping prediction.

2. System Model

In this section, we firstly utilize the APDL language to construct a finite element model of iced conductor, and set parameters such as elastic modulus, Poisson's ratio, and density for each material. Next, the aerodynamic coefficient model is constructed. Finally, based on the above two researches, an aerodynamic excitation model of iced conductor is constructed.

2.1 Finite Element Model

ANSYS parametric design (APDL) language, is a powerful scripting language within the ANSYS software suite. The process of establishing a finite element model typically involves the following steps: defining the geometry of the model, discretizing the model into smaller elements, specifying the material properties within the model, setting boundary conditions and applying external loads, running the solver to compute the model's response, and analyzing and visualizing the results of the solution. A finite element model is established using APDL language, consisting of straight line pole, conductor, post insulator, spacer rod, and metal fitting. The model considers both the translational and rotational movement freedoms of conductors. Therefore, the conductor and spacer rod are simulated by using BEAM188, which can better simulate the actual conditions of conductor during the icing process and ensures the internal node displacement of the conductor cross-section. Considering the constraints between the spacer rod and conductor, the placement of spacer rods is arranged according to the real engineering status of the 500kV transmission line. The transmission line adopts the LGJ-400/50 type conductor, and adopts JZFD4-45400 type spacer rod to divide the spans. The spacer rod is made of aluminum alloy and weighs 7.5kg. In the finite element calculation, the spacer rod is modeled by equivalent modeling method. The conductor is modeled

with a unit of 0.5 m, a conductor span of 45 m, as well as a diameter of 20 mm. Table 1 enumerates the detailed parameters for each material components. For the straight line pole, the bottom surface is designated as fixed. The conductor extremities are configured to a fixed state. The contact between different parts of the conductor is simplified as face-to-face contact.

Temperature and humidity affect the thickness of the ice on the lines [24], while wind speed mainly affects the amplitude of the ice movement [25]. Therefore, based on the finite element model, we construct equivalent icing thickness model and consider the variation models of aerodynamic resistance coefficient, lift force coefficient, and torque coefficient with the angle of the wind attack. The growth of ice accretion on conductors in natural conditions is primarily related to the cumulative duration of meteorological conditions and the impact of meteorological elements. In this paper, meteorological information is precise to local areas in order to predict transmission galloping more accurately. Besides weather information is updated every ten minutes to provide the most up-to-date transmission lines galloping forecast.

Table 1 Material parameter

Name	Density/(kg · m^{-3})	Poission's ratio	Elastic modulus /MPa
Conductor	1 483.32	0.3	59 000
Insulator	2 500	0.25	55 000
Concrete pole	2 440	0.15	39 000
Ice	850	0.3	400

2.2 Aerodynamic Coefficient Model

Under the natural icing state, the iced cross-section of overhead conductor is uncertain, and the actual icing thickness is usually equivalent to the circular cross-section icing thickness of uniform thickness based on ellipse method. In this paper, we consider the N-bundled conductor, which contains a set of sub-conductors $\Gamma = \{a_1, \cdots, a_n, \cdots, a_N\}$. The icing thickness equivalent calculation formula of the n-th sub-conductor at the t-th slot is given by

$$b_n(t) = \sqrt{\frac{d_l^n(\eta(t), \zeta(t)) d_s^n(\eta(t), \zeta(t))}{4}} - \frac{d_n}{2}, \quad (1)$$

where $b_n(t)$ is the equivalent icing thickness of the n-th sub-conductor at the t-th slot. $d_l^n(\eta(t), \zeta(t))$ and $d_s^n(\eta(t), \zeta(t))$ are the major and minor axis of the actual iced cross-section of the n-th sub-conductor at slot t when the temperature is $\eta(t)$ and the humidity is $\zeta(t)$. d_n is the diameter.

Because the iced conductor is mostly irregular shape, it not only suffers resistance, but also lift force and torsion galloping under the action of wind. For the n-th sub-conductor, the aerodynamic resistance, lift force and torque are represented by $F_D^n(t)$, $F_L^n(t)$ and $M^n(t)$, respectively, which are given by

$$F_D^n(t) = \frac{1}{2} C_D^n(t, \alpha) \rho U(t)^2 [d_n + 2b_n(t)], \quad (2)$$

$$F_L^n(t) = \frac{1}{2} C_L^n(t, \alpha) \rho U(t)^2 [d_n + 2b_n(t)], \quad (3)$$

$$M^n(t) = \frac{1}{2} C_M^n(t, \alpha) \rho U(t)^2 [d_n + 2b_n(t)]^2. \quad (4)$$

$U(t)$ and ρ are the wind speed and air density at slot t. $C_D^n(t, \alpha)$, $C_L^n(t, \alpha)$ and $C_M^n(t, \alpha)$ are the coefficients of resistance, lift force and torque of the n-th sub-conductor at slot t, which are associated with the wind attack angle α.

The overall galloping characteristics of the conductor are related to those of each sub-conductor. The coefficients of aerodynamic resistance , lift force and torque of the N-bundled conductor are defined as $C_L(t, \alpha)$, $C_D(t, \alpha)$ and $C_M(t, \alpha)$, respectively, which are given by

$$C_L(t, \alpha) = \frac{1}{N} \sum_{n=1}^{N} C_L^n(t, \alpha), \quad (5)$$

$$C_D(t, \alpha) = \frac{1}{N} \sum_{n=1}^{N} C_D^n(t, \alpha), \quad (6)$$

$$C_M(t, \alpha) = \frac{1}{N} \left[C_{M_S}^N(t, \alpha) + C_{M_L}^N(t, \alpha) + C_{M_D}^N(t, \alpha) \right], \quad (7)$$

where $C_{M_S}^N(t, \alpha)$, $C_{M_L}^N(t, \alpha)$ and $C_{M_D}^N(t, \alpha)$ are the effects of torque, lift force and resistance of each sub-conductor on the overall torque coefficient of the N-bundled conductor. Take the four-bundled conductor as an example, where, $C_{M_S}^N(t, \alpha)$, $C_{M_L}^N(t, \alpha)$ and $C_{M_D}^N(t, \alpha)$ are represented as

$$C_{M_S}^4(t, \alpha) = \sum_{n=1}^{4} C_M^n(t, \alpha), \quad (8)$$

$$C_{M_D}^4(t, \alpha) = \frac{1}{\sqrt{2}} [C_L^1(t, \alpha) - C_L^3(t, \alpha)] \sin\left(\alpha + \frac{\pi}{4}\right)$$
$$+ \frac{1}{\sqrt{2}} [C_L^4(t, \alpha) - C_L^2(t, \alpha)] \cos\left(\alpha + \frac{\pi}{4}\right), \quad (9)$$

$$C_{M_D}^4(t, \alpha) = \frac{1}{\sqrt{2}} [C_D^1(t, \alpha) - C_D^3(t, \alpha)] \sin\left(\alpha + \frac{\pi}{4}\right)$$
$$- \frac{1}{\sqrt{2}} [C_D^4(t, \alpha) - C_D^2(t, \alpha)] \cos\left(\alpha + \frac{\pi}{4}\right). \quad (10)$$

The variation law of aerodynamic resistance coefficient $C_L(t, \alpha)$, lift force coefficient $C_D(t, \alpha)$ and torque coefficient $C_M(t, \alpha)$ with α for the four-bundled conductor is shown in the Figure 1.

2.3 Aerodynamic Excitation Model

The aerodynamic load on the unit node of the iced conductor at the t-th slot can be represented as

$$\left[F_y(t, \alpha), F_z(t, \alpha), F_M(t, \alpha) \right]^T = \frac{1}{2} \rho U(t)^2 (d_n + 2b_n(t))$$
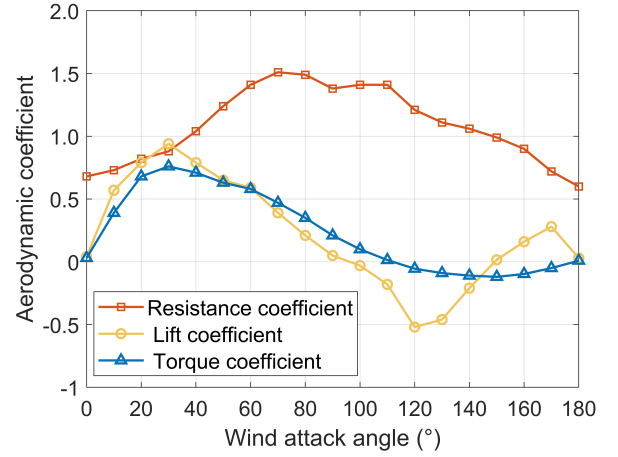

Fig. 1 The variation law of aerodynamic coefficients with the wind attack angle of the four-bundled conductor.

$$\times \left[C_y(t, \alpha), C_z(t, \alpha)(d_n + 2b_n(t)), C_M(t, \alpha) \right]^T. \quad (11)$$

$F_y(t, \alpha)$ and $F_z(t, \alpha)$ are the vertical and horizontal aerodynamic loads on the unit node of the iced conductor. $C_y(t, \alpha)$ and $C_z(t, \alpha)$ are the corresponding coefficients, which are calculated as

$$C_y(t, \alpha) = C_L(t, \alpha) \cos\alpha - C_D(t, \alpha) \sin\alpha, \quad (12)$$
$$C_z(t, \alpha) = C_L(t, \alpha) \sin\alpha + C_D(t, \alpha) \cos\alpha. \quad (13)$$

3. PSO-CGAN-based Iced Transmission Line Galloping Prediction Algorithm

We present the PSO-CGAN-based iced transmission line galloping prediction model, which utilizes the MLP as the discriminator and generator of CGAN. Firstly, the working principle of CGAN is introduced. Then, we optimize the weight parameters in the CGAN loss function by using PSO algorithm to enhance the stability and precision of the discriminator. Finally, the procedures of PSO-CGAN-based iced transmission line galloping prediction are presented.

3.1 Principle of CGAN

In traditional GAN architecture, there is a generator that learns the training set distribution to produce new samples, while a discriminator is employed to differentiate between the generated samples and the actual training set [26], [27]. Based on the difference, the generator and discriminator are adjusted to enhance the discrimination accuracy. However, traditional GANs have the following two shortcomings. First, the virtual samples generated by the generator lack diversity, making it difficult to predict iced transmission line galloping for different scenarios. Second, as the discriminator model being improved, the gradient vanishing problem in the generator model becomes more serious, which makes the entire model difficult to converge and reduces the accuracy of iced transmission line galloping prediction. CGAN,

as a derivative model of GAN, introduces conditions as constraint variables [28], [29], making the model training more purposeful and more suitable for data generation and prediction under specific conditional constraints. In addition, we utilize WasserStein distance to replace the Jensen-Shannon (JS) divergence in the CGAN network, which makes the virtual samples generated by the generator more diverse and closer to the marginal distribution of the original samples. It also reduces the problems of gradient explosion and gradient vanishing, thereby improving the stability of the entire model.

Due to the capability of MLP to effectively address the nonlinear problems, along with strong generalization ability and robust fault tolerance [30], this paper selects MLPs to constitute the CGAN model, as illustrated in Figure 2. The network parameters are denoted as θ_D and θ_G for the discriminator D and the generator G, respectively. During the process of iced transmission line galloping prediction, the information of the conductor to be predicted such as the span and initial wind attack angle acts as input conditions ϕ, which is firstly merged with random disturbances σ and then fed into G. Then, the generator generates the strategy π_{θ_G} and dataset of iced line galloping $G(\sigma|\phi)$. Subsequently, the real sample set of iced line galloping ξ and the results $G(\sigma|\phi)$ generated by the generator are respectively merged with the input conditions ϕ, and then fed into the discriminator D. The discriminator D outputs the galloping prediction strategy π_{θ_D}, judges the similarity between the actual and generated samples by computing the distribution distance, and judges whether the generated samples meet the conditions ϕ.

Traditional CGAN uses the JS distance to describe the error between real and generated sample data. During the early stages of training, when the generating capability of the generator is insufficient, real samples and generated samples may be entirely independent. Consequently, the JS distance between the two sample data distributions remains constant. This can lead to the training stagnation and the problem of gradient vanishing during the updating process of the discriminator network parameters. To effectively address the instability issue in CGAN training, the WasserStein distance is employed to obtain the disparity between the actual and generated distributions [31]. It makes the generated samples more diverse and closer to the marginal distribution of the actual samples, which prevents gradient vanishing during generator network parameter updating, thus enhancing the overall stability of the model [32].

The WasserStein distance between the distribution of sample generated by the generator $p(G(\sigma|\phi))$ and the real sample distribution $p(\xi)$ is given by

$$W(p(G(\sigma|\phi)), p(\xi)) = \inf_{\gamma \sim \Pi(p(G(\sigma|\phi)), p(\xi))} E_{(x,y) \sim \gamma} \left[\| x - y \| \right], \quad (14)$$

where $\Pi(p(G(\sigma|\phi)), p(\xi))$ represents the joint probability distribution with $p(G(\sigma|\phi))$ and $p(\xi)$ as marginal distributions. For each possible joint distribution γ, a ac-
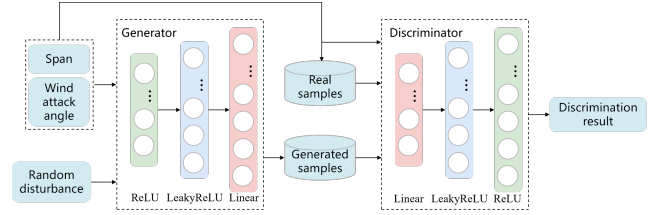

Fig. 2   CGAN model.

tual sample $x \in \xi$ and a generated sample $y \in G(\sigma|\phi)$ can be obtained through sampling, and the distance between x and y, i.e., $\| x - y \|$, is then calculated. Subsequently, the expectation of $\| x - y \|$ under this joint distribution is given by $E_{(x,y) \sim \gamma} [\| x - y \|]$. The infimum $\inf_{\gamma \sim \Pi(p(G(\sigma|\phi)), p(\xi))} E_{(x,y) \sim \gamma} [\| x - y \|]$ is defined as the Wasserstein distance between $p(G(\sigma|\phi))$ and $p(\xi)$.

The loss functions L_G and L_D of the generator and discriminator are adjusted by utilizing the WasserStein distance. With the adjusted loss functions, the generator and discriminator enhance the model learning capability through mutual adversarial training. The loss functions L_G and L_D of the CGAN generator and discriminator are given by

$$L_G = -E_{\sigma \sim p(\sigma)} [\log (1 - D(G(\sigma|\phi)|\phi))], \quad (15)$$

$$L_D = -E_{\xi \sim p(\xi)} \left[\log D(\xi|\phi) \right] + E_{\sigma \sim p(\sigma)} [\log (1 - D(G(\sigma|\phi)|\phi))], \quad (16)$$

where $E_{\sigma \sim p(\sigma)}$ represents the expectation of the disturbance distribution $p(\sigma)$, and $E_{\xi \sim p(\xi)}$ represents the expectation of the real sample distribution $p(\xi)$.

Based on (15) and (16), the loss function L_{CGAN} of CGAN is given by

$$L_{\text{CGAN}} = E_{\xi \sim p(\xi)} \left[\log D(\xi|\phi) \right] + E_{\sigma \sim p(\sigma)} [\log (1 - D(G(\sigma|\phi)|\phi))]. \quad (17)$$

To improve the precision of the CGAN model, numerical deviation L_{qd} and galloping morphology deviation L_{fd} are constructed to adjust L_{CGAN}. The numerical deviation L_{qd} is calculated as the mean square error between x and y, which is given by

$$L_{\text{qd}} = \frac{1}{V} \sum_{v=1}^{V} (y(v) - x(v))^2, \quad (18)$$

where V is the sample quantity in the actual sample set ξ and the generated sample set $G(\sigma|\phi)$. $x(v)$ and $y(v)$ are the v-th element in ξ and $G(\sigma|\phi)$, respectively.

The supremum of $\| x - y \|$ is denoted as $\sup_{(x,y) \sim \gamma} \| x - y \|$. The galloping morphology deviation L_{fd} can be expressed as

$$L_{\text{fd}} = 1 - \frac{W(p(x), p(y))}{\sup_{(x,y) \sim \gamma} \| x - y \|}, \quad (19)$$

where $W(p(x), p(y))$ is the Wasserstein distance between

the actual sample distribution $p(x)$ and the generated sample distribution $p(y)$.

Therefore, the corrected loss function of CGAN can be represented as

$$L(G, D) = L_{\text{CGAN}} + \omega_{\text{qd}} L_{\text{qd}} + \omega_{\text{fd}} L_{\text{fd}}, \tag{20}$$

where ω_{qd} and ω_{fd} are the weight parameters of the numerical deviation L_{qd} and the galloping morphology deviation L_{fd}, respectively.

Based on the corrected loss function $L(G, D)$, the generator network parameter θ_G and the discriminator network parameter θ_D are updated as

$$\theta_G = \theta_G - \rho_G \nabla_{\theta_G} \log \pi_{\theta_G} \partial(G(\sigma|\phi)), \tag{21}$$

$$\theta_D = \theta_D - \rho_D \nabla_{\theta_D} \log \pi_{\theta_D} \partial(\xi), \tag{22}$$

where ρ represents the learning rate of the network and ∇ denotes the gradient function.

3.2 PSO-based CGAN Parameter Optimization

In CGAN, the numerical deviation L_{qd} reflects the numerical accuracy of the generated curves, including the similarity of average value, maximum value and minimum value to the real curves. The galloping morphology deviation L_{fd} reflects the morphology similarity of the generated curves, including the similarity of the fluctuation range and variation trend to the real curves. Generally, smaller values for the weight parameters of the numerical deviation and the galloping morphology deviation indicate lower requirements on the numerical distribution and galloping morphology characteristics of the generated curves, emphasizing the overall performance of CGAN and leading to unreliable judgments by the discriminator. Conversely, larger values for these weight parameters indicate higher requirements on the numerical distribution and galloping morphology characteristics of the generated curves, neglecting the overall performance of the CGAN and resulting in increased network discrimination latency. Therefore, we utilize the PSO to explore appropriate weight parameters of numerical deviation and galloping morphology deviation, ensuring high accuracy and stability of the discriminator.

(1) Parameters initialization

We stipulate the PSO to run for a maximum of $k_{\max}$ iterations, initialize the iteration count as $k = 1$, and initialize the number of particles as S. The position of each particle represents a feasible soluti on, which corresponds to a set of values of the weight parameters for the numerical deviation and the galloping morphology deviation. The information of each particle can be represented by a 2-dimensional vector. Specifically, the position is denoted as $Xs = \{\omega_{\text{qd}}^s, \omega_{\text{fd}}^s\}^T$, and the velocity is denoted as $Vs = \{V_s^1, V_s^2\}^T$, where s is the particle number. The velocity indicates the direction in which the particle moves in the search space, determining the particle's next position.

(2) Fitness value calculation

The solution is assessed by computing the fitness value $H_s(X_s)$ of the position of particle s. The higher the fitness value is, and the closer the current particle position is to the optimal solution, the better the corresponding weight parameters are. Similarly, the discrimination accuracy of the discriminator will be higher. With the updated CGAN network, a new set of generated samples $G'(\sigma|\phi)$ is obtained. Therefore, the fitness value of the position X_s of particle s is given by

$$H_s(X_s) = \frac{1}{W(p(\xi), p(G'(\sigma|\phi)))}. \tag{23}$$

(3) Particle state update

During the optimization process, the best position of the current particle, i.e., individual extremum P_k^{best}, and the best position of all particles, i.e., global extremum U^{best}, are dynamically tracked. Denote the fitness value of the s-th particle after k iterations as $H_s(k)$. If $H_s(k) > H_{P^{\text{best}}}$ and $H_s(k) > H_{U^{\text{best}}}$, update both the individual and global best position. If $H_s(k) > H_{P^{\text{best}}}$ and $H_s(k) \leq H_{U^{\text{best}}}$, only update the individual best position of particle. Here, $H_{P^{\text{best}}}$ and $H_{U^{\text{best}}}$ represent the fitness values of the historical best position of the current particle, i.e, P^{best}, and that of all particles, i.e., U^{best}. The position and velocity of particle s are given by

$$\begin{cases} V_s^{k+1} &= \omega V_s^k + c_1 r_1 \left(P_s^k - X_s^k \right) + c_2 r_2 \left(P_g^k - X_s^k \right), \\ X_s^{k+1} &= X_s^k + V_s^{k+1}, \end{cases}$$
$$\tag{24}$$

where ω represents the inertia weight of velocity. c_1 and c_2 represent acceleration coefficients. r_1 and r_2 represent random numbers within $[0,1]$. P_s^k and P_g^k denote the best solutions of the s-th particle and all particles in the k-th iteration process, respectively.

(4) Output the optimal weight parameters

The algorithm determines whether the maximum number of iterations has been reached, i.e., $k = k_{\max}$. If the maximum number of iterations is reached, the algorithm outputs the global optimal positions U^{best} of all particles, and terminates. Meanwhile, the weight parameters of numerical deviation and galloping morphology deviation are optimized. Otherwise, $k = k + 1$.

3.3 Implementation Steps of PSO-CGAN-based Iced Transmission Line Galloping Prediction

The overall implementation steps of the proposed algorithm are illustrated in Figure 3 and Algorithm 1 , and are summarized as follows.

Step 1: Initialize the parameters of the CGAN generator G and discriminator D, set the maximum number of iterations as $m_{\max}$, and initialize the iteration count as $m = 1$.

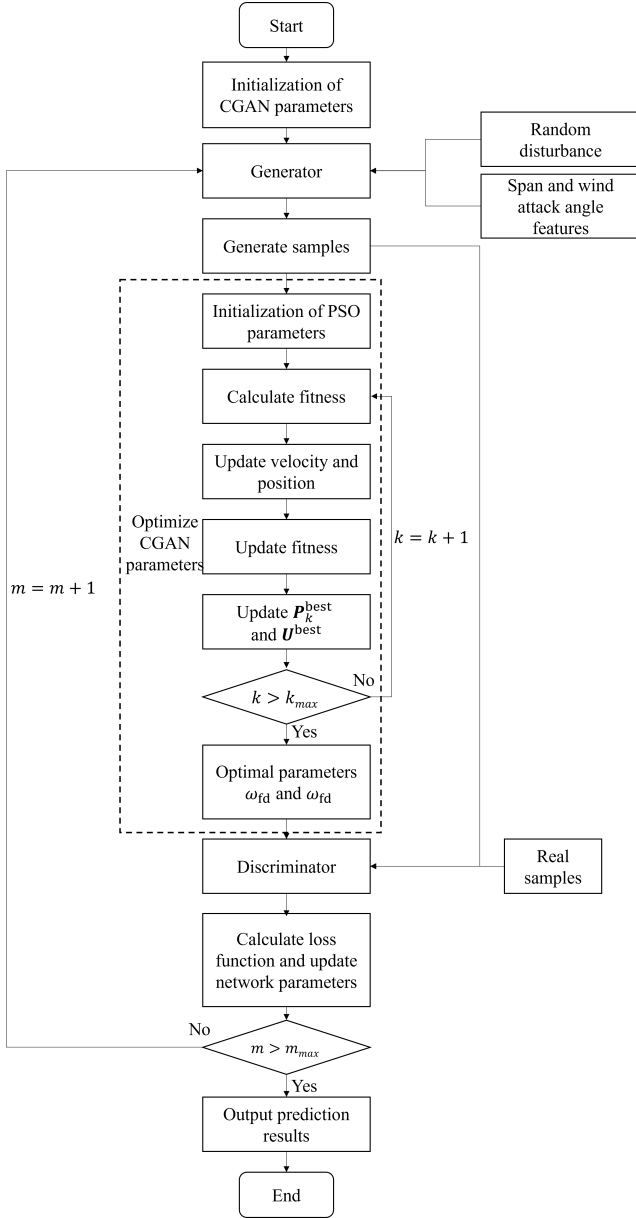**Step 2:** Use the set of span and initial wind attack

Fig. 3   Implementation procedures of the proposed algorithm.

angle as input conditions ϕ, and input them into the generator G along with random disturbances σ to generate iced transmission line galloping samples $G(\sigma|\phi)$.

Step 3: Input the actual and generated samples as well as input conditions into the discriminator. The discriminator judges whether the actual and generated samples are similar, and whether the generated samples meet the conditions. Then, calculate the loss functions of the discriminator and generator according to (15) and (16), respectively.

Step 4: Initialize the parameters of the PSO, including the number of particles S, particle positions X_s, particle velocities V_s, maximum number of iterations $k_{\max}$, and iteration count $k = 1$.

Step 5: Calculate the fitness value $H_s(X_s)$ of the particle based on the weight parameters of numerical deviation

and galloping morphology deviation to assess the quality of the solution, i. e. (23).

Step 6: Update the individual and global best positions based on (24). If $H_s(k) > H_{\boldsymbol{P}\text{best}}$ and $H_s(k) > H_{\boldsymbol{U}\text{best}}$, update both the individual and global best position. If $H_s(k) > H_{\boldsymbol{P}\text{best}}$ and $H_s(k) \leq H_{\boldsymbol{U}\text{best}}$, only update the individual best position of particle.

Step 7: Update $k = k + 1$. Execute Steps 5 and 6 until $k > k_{\max}$. Output the optimal weight parameters of numerical deviation and galloping morphology deviation.

Step 8: Based on the optimal weight parameters, calculate the corrected loss function based on (20), and update the network parameters of CGAN based on (21) and (22) to optimize the network.

Step 9: Update $m = m + 1$. Execute Steps 2-8 until $m > m_{\max}$. Output the prediction results.

Algorithm 1 PSO-CGAN-based Iced Transmission Line Galloping Prediction

---

1: **Initialization:** Initialize the particle positions X_s and particle velocities V_s. Set $m = 1$.
2: **While** $m \leq m_{\max}$
3:     Input the set of span and initial wind attack angle into the generator G along with random disturbances σ.
4:     Input the actual and generated samples as well as input conditions into the discriminator.
5:     Calculate the loss functions of the discriminator and generator based on (15) and (16).
6:     Set $k = 1$.
7:     **While** $k \leq k_{\max}$
8:       **For** $s=1,2,...,S$ **do**
9:        Calculate the fitness value $H_s(X_s)$ of the particle based on (23).
10:        Update the individual and global best positions based on (24).
11:       **End for**
12:       Set $k = k + 1$.
13:     **End while**
14:     Calculate the corrected loss function based on (20).
15:     Update the network parameters of CGAN based on (21) and (22).
16:     Set $m = m + 1$.
17: **End while**

3.4   Complexity Analysis

The computational complexity of PSO-CGAN is composed of three parts. The first part is the data sample generated by the CGAN generator network. The computational complexity of the generator network is $O(e_1 \mu_1^2)$, where e_1 is the number of neurons and μ_1 is the number of layers in the generator network. The second part is the optimization of the discriminator network parameters' weight values using PSO. The computational complexity of optimizing parameters with PSO is $O(Sk_{\max}(1 + 1 + 1))$. The third part is the discriminator network distinguishing between generated samples and real samples. The computational complexity of the discriminator network is $O(e_2 \mu_2^2)$, where e_2 is the number of neurons and μ_2 is the number of layers in the discriminator network. Therefore, the total computational

complexity is $O(m_{max}\{e_1\mu_1{}^2 + 3Sk_{max}e_2\mu_2{}^2\})$.

4. Simulation

Considering the difficulty in actual data collection, this paper firstly employs Fluent [33] software for the galloping simulation of a iced four-bundled conductor, generating a dataset of the conductor galloping. Subsequently, the impacts of initial wind attack angle, wind speed, and icing thickness on the conductor galloping are analyzed based on the dataset and compared with the actual situation. Then, preprocessing is performed on the simulation dataset. Train the CGAN prediction model by using the training samples and used to generate prediction results. Finally, the efficacy of PSO-CGAN is confirmed by comparing its prediction accuracy against that of the following four algorithms.

(1) The prediction of ice-covered dancing on transmission line based on back propagation (BP) neural network. This algorithm typically consists of an input layer, hidden layers, and an output layer. During forward propagation, input features are processed by the network's hidden layers, and then BP adjusts weights and biases to minimize prediction errors [34].

(2) The prediction of ice-covered dancing on transmission line based on the support vector machine (SVM) model utilizes historical data, including meteorological conditions and line parameters, to predict the likelihood or amplitude of galloping [35].

(3) The prediction of ice-covered dancing on transmission line based on GAN employs a generator to create realistic samples resembling actual galloping data and a discriminator to evaluate the differences between generated and observed icing galloping data [36].

(4) GA is used to optimize SVM parameters and enhance galloping prediction performance in the prediction of ice-covered dancing on transmission line based on GA-SVM, while SVM may require more tuning to avoid overfitting, especially with limited training data [37].

4.1 Simulation Result

Fluent software is utilized to simulate the aerodynamic coefficients of a four-bundled conductor with the conductor type of LGJ-400/50. The spacing between sub-conductors is 450 mm, and the radius is 13.8 mm. The conductor model is created in Gambit software, and the flow field is set to a size of 2m×2m. Unstructured grid is used for grid division. Transient analysis is conducted using Fluent software, and the solver is set to the simple algorithm, Spalart-Allmaras turbulence model, and second-order implicit scheme. The time step is set to 0.001 s, and a total of 200 time steps are simulated. The wind angle of attack α varies from 0° to 180° in increments of 10° in counterclockwise direction. A total of 2500 data points are obtained from the Fluent simulations, as shown in Table 2, where 0 indicates no galloping and 1 indicates galloping.

Table 2 Simulation dataset.

Icing thickness /mm	Wind speed /(m·s^{-1})	Initial wind attack angle/°	Galloping	Galloping Amplitude /m	Torsion angle/°
5	3	10	0	/	/
5	3	90	0	/	/
5	4	90	0	/	/
5	4	10	1	0.6	0.08
5	9	30	1	1.5	0.16
5	9	30	1	1.5	0.16
8	9	30	1	1.9	0.17
8	12	60	1	3.5	0.45
12	12	60	1	3.9	0.51
12	12	60	1	4.1	0.52
...	...	...	...	...	...

4.1.1 The Impact of Icing Thickness on Galloping

Figure 4 shows the variations of galloping amplitude and torsion angle with icing thicknesses under a wind attack angle of 30° and various wind speeds. The solid line represents the former and the dotted line represents the latter. It is noticeable that as the icing thickness and wind speed escalate, there is a corresponding rise in both the galloping amplitude and torsion angle. For example, when the wind speed is maintained at 12 m/s, as the icing thickness increases from 0 mm to 12 mm, the galloping amplitude increases by a factor of 12.3, while the torsion angle increases by 34.2%. It indicates that an increased icing thickness leads to a more pronounced increase in the torsion angle, resulting in more severe torsion under the same wind speed. Similarly, at an icing thickness of 6 mm, when the wind speed rises from 4 m/s to 12 m/s, the torsion angle has an increase of 35.7%. Meanwhile, the galloping amplitude increases from 0.8 m to 3.8 m, a 4.8-fold increase. It is noticeable that an increase in wind speed under the same icing thickness results in a greater increase in galloping amplitude, leading to a more severe galloping of the conductor, which is consistent with the actual situation.

4.1.2 The Impact of Wind Speed on Galloping

Figure 5 illustrates the variations of galloping amplitude with wind speed under various icing thicknesses for an initial wind attack angle of 30°. It is noticeable that as the wind speed reaches 4 m/s, the iced four-bundled conductor reaches the galloping condition, and the galloping amplitude begins to increase. After the wind speed exceeds 20 m/s, the galloping amplitude experiences a significant decline. Moreover, under the same wind speed, an increase in icing thickness exacerbates the galloping amplitude, but the magnitude of exacerbation is relatively small. Specifically, when the wind speed is 20 m/s, the galloping amplitude only increases by 17% when the icing thickness increases from 5 mm to 12 mm. Furthermore, under the same icing thickness, an increase in wind speed exacerbates the galloping amplitude with a large exacerbation magnitude. For instance, when the
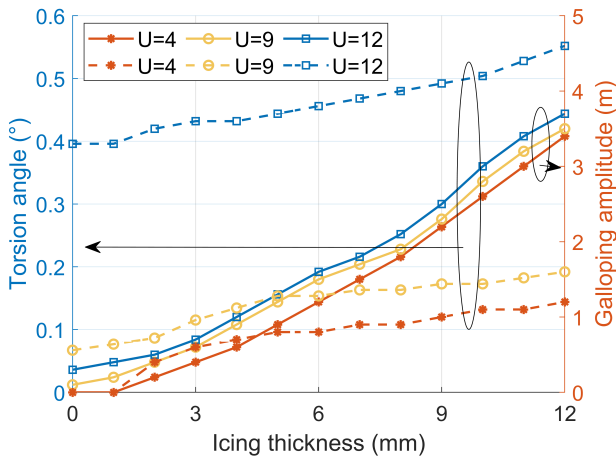
Fig. 4   Variations of galloping amplitude and torsion angle with icing thickness at different wind speeds.

icing thickness is 12 mm, increasing the wind speed from 5 m/s to 20 m/s leads to a 6.7-fold increase in the galloping amplitude. Overall, these observations conform to the actual scenario.
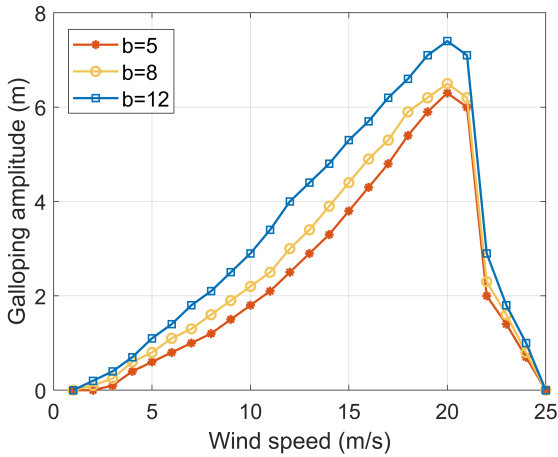

Fig. 5   Variations of galloping amplitude with wind speeds at different icing thickness.

4.1.3   The Impact of Wind Attack Angle on Galloping

The galloping size and shape also depend on the angle formed by the wind and the conductor's axis, i.e., initial wind attack angle. Table 3 shows the galloping amplitudes for iced conductors at different wind attack angles under conditions of an 8 m/s wind speed and a conductor span of 200 m.

The table shows that as the initial wind attack angle increases, the corresponding galloping amplitude also increases, reflected in vertical displacement, horizontal displacement, and torsion angle. The galloping amplitude is observed to be zero at initial wind attack angles of 0° and

Table 3   Galloping amplitudes of four-bundled conductor at different wind attack angles.

Initial wind attack angle/(°)	Vertical displacement/m	Horizontal displacement/m	Torsion angle/(°)
0	0	0	0
30	0.37	0.48	0.17
60	8.05	3.41	0.51
90	0	0	0

90°. The reason behind is that when the initial wind attack angle is 0°, the wind direction is parallel to the conductor, minimizing induced vibrations. Similarly, the wind direction being perpendicular to the conductor, the lift force is reduced and converges towards zero, resulting in a limited propensity for galloping. Furthermore, a notable disparity exists in galloping amplitude when the initial wind attack angle is 30° and 60°, which indicates the substantial impact of different wind attack angles on conductor galloping.

4.2   Algorithm Comparison

In this paper, a subset of the galloping simulation dataset obtained in Section 4.1 is selected for training the prediction model, while the remaining data is used for testing. The proposed prediction process for iced conductor galloping is depicted in Figure 6. The specific steps are outlined as follows:
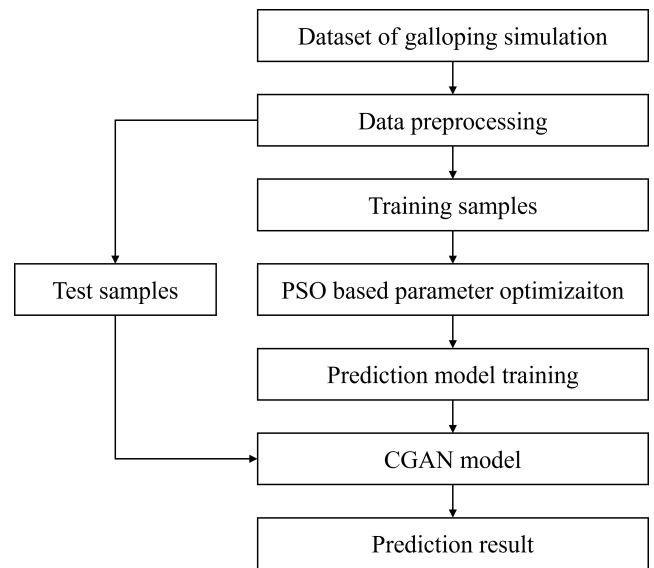

Fig. 6   Prediction flow chart.

Step 1: Randomly select 70% of the galloping and non-galloping data,, i.e., a total of 1750 data samples, from the simulated galloping dataset obtained in Section 4.1, to be utilized as the training data for the CGAN iced galloping prediction model. It ensures a sufficient amount of data for prediction accuracy enhancement.

Step 2: Carry out data preprocessing on the original galloping simulation dataset. Due to the different orders of

magnitude for the input variables, it is necessary to normalize the sample data. The normalization formula is given by

$$x = \frac{x_0 - x_{\min}}{x_{\max} - x_{\min}} \tag{25}$$

where x_0 and x are the data values before and after normalization, respectively. $x_{\max}$ and $x_{\min}$ are the greatest and least data values before normalization.

Step 3: The optimal weight parameters ω_{qd} and ω_{fd} for CGAN are obtained by using PSO. Then, the CGAN-based iced line galloping prediction model is trained based on the gradient descent method.

Step 4: The remaining 750 data samples from Step 1 are used as test data for the CGAN-based iced line galloping prediction model. The original data is compared with the predicted results outputted by the model to determine the accuracy of the PSO-CGAN-based galloping prediction.

Table 4 shows the comparison of prediction accuracy of different algorithms and Table 5 presents few samples from the generated dataset. The PSO-CGAN model achieves an accuracy rate of 98.48% in identifying iced line galloping, which outperforms BP, SVM, GAN and GA-SVM by 47.25%, 9.11%, 6.72% and 2.00%, respectively. The reason for the superior performance of the proposed algorithm lies in two aspects. Firstly, by utilizing the WasserStein distance, the algorithm effectively addresses the instability in training CGAN network, ensuring that the generated data closely resembles the distribution of real samples. Secondly, the algorithm incorporates PSO to optimize the weight parameters of CGAN, which strikes a balance between feature requirements and overall network performance, and improves the accuracy, stability, and convergence speed of model.

Table 4   The comparison of prediction accuracy of different algorithms.

Algorithm	BP	SVM	GAN	GA-SVM	PSO-CGAN
Accuracy/%	66.88	90.26	92.28	96.54	98.48

Table 5   Samples from the generated dataset

Icing thickness /mm	Wind speed /(m·s⁻¹)	Initial wind attack angle/°	Galloping	Galloping amplitude /m	Torsion angle/°
5	4	30	1	0.8	0.11
8	9	30	1	1.9	0.16
8	12	30	1	3.7	0.48
12	9	60	1	3.3	0.41
12	4	90	0	/	/
...	...	...	...	...	...

Figure 7 illustrates loss functions of the generator and discriminator versus iteration. It can be observed that, during the initial training phase, the loss function of the generator gradually increases while the loss function of the discriminator decreases, indicating the poor generation capability of the generator at this stage. The networks are currently

in the adversarial phase, and the prediction model exhibits weak prediction ability. After 2000 iterations, the model reaches a state of convergence. By 6000 iterations, the networks stabilize, indicating that the discriminator is no longer able to accurately differentiate between real and generated samples. The generator successfully generates a falsely generated data distribution approximating the real one, enabling the prediction model to accurately predict results based on input data.
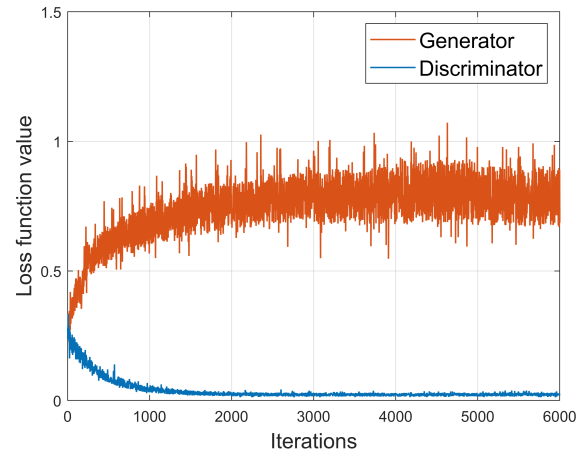

Fig. 7   The loss functions versus iterations.

Figure 8 shows the box plot of deviation between the iced conductor galloping amplitude predicted by different prediction models and the original data. Compared with BP, SVM, GAN and GA-SVM, the median of the galloping amplitude deviation of the proposed algorithm is reduced by 79.68%, 62.13%, 52.45% and 40.57%, respectively, and the maximum deviation is reduced by 83.95%, 71.36%, 68.95% and 55.03%, respectively. By using WasserStein distance to measure the disparity between the actual and the generated distributions, the proposed algorithm solves training instability resulted by the gradient disappearance in CGAN network training. Therefore, the generated false data are closer to the actual data distribution, and the prediction result is closest to the original data. BP is mainly suitable for supervised learning tasks such as classification and regression and the galloping amplitude prediction ability is poor.

Figure 9 shows the absolute value of the average torsion angle prediction deviation of different prediction models versus iterations. As the iterations increase, the absolute values of the average torsion angle prediction deviation of the four prediction models gradually decrease, and the proposed algorithm has the fastest convergence speed. Compared with BP, SVM, GAN and GA-SVM, the convergence speed of the proposed algorithm increases by 31.24%, 22.23%, 18.75% and 9.87%, respectively. The proposed algorithm uses PSO to search for appropriate weight parameters, which improves the accuracy and stability of the network and is conducive to the learning of the network. At the same time, PSO has
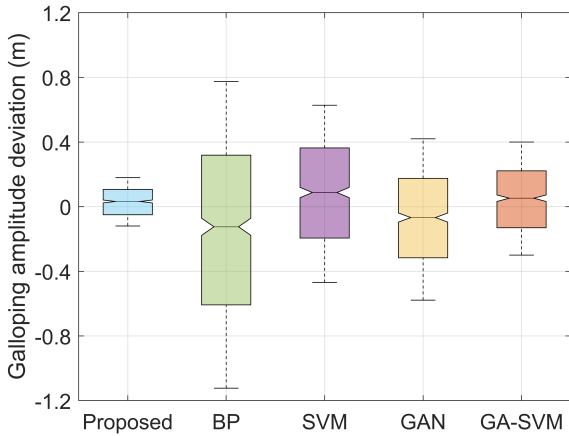
Fig. 8 Deviation between the galloping amplitude predicted by different prediction models and the original data.

the memory function and accelerates the convergence of the prediction model.
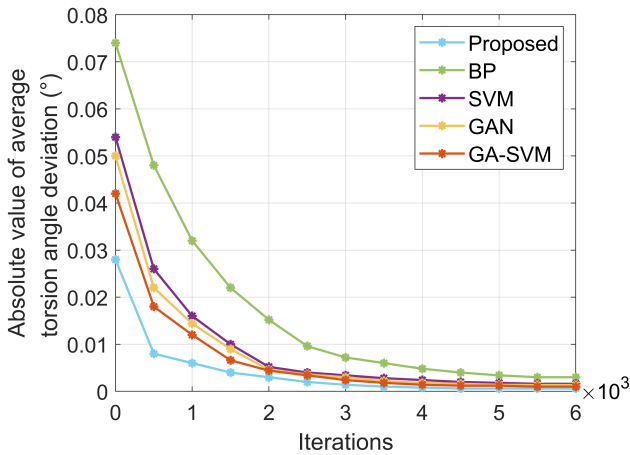

Fig. 9 The absolute value of the average torsion angle prediction deviation versus iterations.

5. Conclusion

A PSO-CGAN-based iced transmission line galloping prediction model was presented in this paper. First, we establish the finite element model and the aerodynamic coeffcient model of the iced conductor. The dynamic response of LGJ-400/50 type conductor under different conditions such as span and wind speed was simulated by the finite element software, and a dataset with 2500 data samples was obtained. Then, based on the PSO-CGAN algorithm, the optimal weight parameters of CGAN were obtained by using PSO, and the iced transmission line galloping prediction model was constructed. The initial wind attack angle, wind speed and span were input to the model to predict

the galloping condition. Next, according to the galloping characteristics of the conductor, the influence of different wind speeds, initial wind attack angle and icing thickness on galloping was studied. Finally, we verified the effective performance of the proposed model in terms of prediction accuracy through simulation. The simulation results show that compared with BP, SVM, GAN and GA-SVM models, the accuracy of the proposed algorithm was improved by 47.25%, 9.11%, 6.72% and 2.00%, respectively. In the future, we will explore more data enhancement techniques to enhance the noise resistance, and provide more reliable galloping prediction services for the stable operation of the power grid.

Acknowledgments

References

[1] M. Tariq, M. Ali, F. Naeem, and H.V. Poor, "Vulnerability assessment of 6g-enabled smart grid cyber–physical systems," IEEE Internet of Things Journal, vol.8, no.7, pp.5468–5475, 2021.

[2] T. Tan, C. Duan, X. Liu, D. Fan, Z. Ye, K. Xie, Q. Chai, Y. Tian, and J. Zhang, "Research on monitoring the transmission line tension and galloping based on FBG fitting sensor," IEEE Transactions on Instrumentation and Measurement, vol.71, pp.1–8, 2022.

[3] J. Yang, B. Liu, B. Zhao, and Y. Liu, "Method for the development of galloping distribution maps for overhead transmission lines," IEEE Transactions on Power Systems, vol.36, no.6, pp.5956–5958, 2021.

[4] M. Tariq, M. Adnan, G. Srivastava, and H.V. Poor, "Instability detection and prevention in smart grids under asymmetric faults," IEEE Transactions on Industry Applications, vol.56, no.4, pp.4510–4520, 2020.

[5] Y. Xian, L. Zhou, J. Jiang, B. Wang, H. Huo, and P. Liu, "A distributed efficient blockchain oracle scheme for internet of things," IEICE Transactions on Communications, vol.PP, no.99, pp.1–11, 2024.

[6] J. Si, X. Rui, B. Liu, L. Zhou, and S. Liu, "Study on a new combined anti-galloping device for UHV overhead transmission lines," IEEE Transactions on Power Delivery, vol.34, no.6, pp.2070–2078, 2019.

[7] Q. Zhao, I. Taniguchi, M. Nakamura, and T. Onoye, "Magic line: An integrated method for fast parts counting and orientation recognition using industrial vision systems," IEICE Transactions on Fundamentals of Electronics, Communications and Computer Sciences, vol.103, no.7, pp.928–936, 2020.

[8] Z. Mou, B. Yan, H. Yang, K. Wu, C. Wu, and X. Yang, "Study on anti-galloping efficiency of rotary clamp spacers for eight bundle conductor line," Cold Regions Science and Technology, vol.193, p.103414, 2022.

[9] M. Tariq and H.V. Poor, "Electricity theft detection and localization in grid-tied microgrids," IEEE Transactions on Smart Grid, vol.9, no.3, pp.1920–1929, 2018.

[10] J. Si, X. Rui, L. Bin, L. Zhou, and S. Liu, "Development of a wind spoiler anti-galloping device for bundle conductors of uhv overhead transmission lines," IEEE Transactions on Power Delivery, vol.35, no.3, pp.1348–1356, 2020.

[11] J.Y. Zheng, Q.H. Shen, and X.H. Liu, "Investigation into the galloping characteristics of multispan iced covered conductors," IEEE Access, vol.10, pp.64580–64600, 2022.

[12] B. Huo, X. Liu, and S. Yang, "Galloping of iced transmission lines considering multi-torsional modes and experimental validation on a

continuous model," IEEE Transactions on Power Delivery, vol.37, no.4, pp.3016–3026, 2022.

[13] W. Lou, Z. Wen, and H. Liang, "A multi-objective optimization framework for anti-galloping of UHV transmission lines using MTTMD based on weighted satisfaction," IEEE Transactions on Power Delivery, vol.37, no.1, pp.249–257, 2022.

[14] G. Diana, A. Manenti, and S. Melzi, "Energy method to compute the maximum amplitudes of oscillation due to galloping of iced bundled conductors," IEEE Transactions on Power Delivery, vol.36, no.5, pp.2804–2813, 2021.

[15] S. Sun, Z. Cao, H. Zhu, and J. Zhao, "A survey of optimization methods from a machine learning perspective," IEEE Transactions on Cybernetics, vol.50, no.8, pp.3668–3681, 2020.

[16] J. Wang, X. Xiong, N. Zhou, Z. Li, and W. Wang, "Early warning method for transmission line galloping based on SVM and AdaBoost bi-level classifiers," IET Generation, Transmission & Distribution, vol.10, no.14, pp.3499–3507, 2016.

[17] L. Yang, L. Li, J. Guo, X. Huai, X. Xu, and J. Xun, "Galloping early warning technology of transmission lines based on RBF neural network," 2019 IEEE 3rd Conference on Energy Internet and Energy System Integration (EI2), Changsha, China, pp.2374–2378, 2019.

[18] L. Zhang, B. Liu, B. Zhao, X. Fei, and Y. Cheng, "Forecasting for the risk of transmission line galloping trip based on BP neural network," Geo-Spatial Knowledge and Intelligence, ed. H. Yuan, J. Geng, and F. Bian, Singapore, pp.168–175, Springer Singapore, 2017.

[19] C. Shi, B. Pan, X. Guo, Q. Li, L. Zhang, and F. Zhong, "Application of generating confrontation network in image completion," Journal of Frontiers of Computer Science and Technology, vol.13, no.8, pp.1402–1410, 2019.

[20] X. Liang, L. Lee, W. Dai, and E.P. Xing, "Dual motion gan for future-flow embedded video prediction," 2017 IEEE International Conference on Computer Vision (ICCV), pp.1762–1770, 2017.

[21] W.Q. Wang Wei, Yang Hao *et al.*, "Mechanical characteristics of tower and conductor jump height of UHV DC lines in ultra-heavy ice zone after ice-shedding," Journal of Chongqing University, vol.PP, no.99, pp.1–10, 2024.

[22] Y.Y. Liu Yating, Yang Ming *et al.*, "Transitional-weather-considered day-ahead wind power forecasting based on multi-scene sensitive meteorological factor optimization and few-shot learning," High Voltage Engineering, vol.49, no.7, pp.2972–2982, 2023.

[23] Y.T. Lu Danhong, Fan Wenyao *et al.*, "Anomaly detection of power load data based on transformer and generative adversarial networks," Electric Power Engineering Technology, vol.43, no.1, pp.157–164, 2024.

[24] Z. Xu, S. Song, L. Zhao, and X. Li, "Opgw icing monitoring method based on phase difference between temperature curves," IEEE Transactions on Power Delivery, vol.39, no.2, pp.1303–1306, 2024.

[25] B. Zhao, Y.f. Cheng, J.c. Wang, B. Liu, and Y.s. Chen, "Effect of wind gradient on the nonlinear dynamic properties of galloping of iced ultra-high-voltage long-span transmission lines," 2018 5th International Conference on Information Science and Control Engineering (ICISCE), pp.737–744, 2018.

[26] K. Dietz, M. Seufert, and T. Hoßfeld, "Want more WANs? comparison of traditional and gan-based generation of wide area network topologies via graph and performance metrics," IEEE Transactions on Network and Service Management, vol.21, no.1, pp.4–19, 2024.

[27] M. Yasuda, S. Yoshida, and M. Muneyasu, "New performance evaluation method for data embedding techniques for printed images using mobile devices based on a GAN," IEICE Transactions on Fundamentals of Electronics Communications and Computer Sciences, vol.E106A, no.3, pp.481–485, 2023.

[28] D. Xiaochong, S. Yingyun, and P. Tianjiao, "Day-ahead scenario generation of renewable energy based on conditional gan," Proceedings of the CSEE, vol.40, no.17, pp.5527–5536, 2020.

[29] T. Srikotr and K. Mano, "Vector quantization of speech spectrum based on the vq-vae embedding space learning by gan technique," IEICE Transactions on Fundamentals of Electronics Communica-

tions and Computer Sciences, vol.E105A, no.4, pp.647–654, 2022.

[30] W. Hu and Y.X. Guo, "An evolutionary multilayer perceptron-based large-signal model of GaN HEMTs including self-heating and trapping effects," IEEE Transactions on Microwave Theory and Techniques, vol.70, no.2, pp.1146–1156, 2022.

[31] W. Hu, T. Wang, and F. Chu, "Fault feature recovery with wasserstein generative adversarial imputation network with gradient penalty for rotating machine health monitoring under signal loss condition," IEEE Transactions on Instrumentation and Measurement, vol.71, pp.1–12, 2022.

[32] W. Fu, Y. Chen, H. Li, X. Chen, and B. Chen, "Imbalanced fault diagnosis using conditional wasserstein generative adversarial networks with switchable normalization," IEEE Sensors Journal, vol.23, no.23, pp.29119–29130, 2023.

[33] Z. Liu, L. Deng, M. Liu, and B. Liu, "Analysis of galloping tension characteristics at suspension points of continuous span transmission lines," 2020 10th International Conference on Power and Energy Systems (ICPES), pp.13–18, 2020.

[34] H. Yin, Q. Wu, C. Liu, L. Xia, C. Zhang, and X. Wang, "Research on the reconstruction of galloping curve of transmission line based on BP neural network," 2023 International Conference on Distributed Computing and Electrical Circuits and Electronics (ICDCECE), Ballar, India, pp.1–6, 2023.

[35] K. Wang, J. Sun, C. Wu, and Y. Yu, "Conductor galloping detection on imbalanced dataset: SVM with smart sampling," 2020 IEEE Power & Energy Society General Meeting (PESGM), Montreal, QC, Canada, pp.1–5, 2020.

[36] Z. Zhang and M. Wu, "Predicting real-time locational marginal prices: A gan-based approach," IEEE Transactions on Power Systems, vol.37, no.2, pp.1286–1296, 2022.

[37] J. Ruan, H. Jiang, X. Li, Y. Shi, F.T.S. Chan, and W. Rao, "A granular ga-svm predictor for big data in agricultural cyber-physical systems," IEEE Transactions on Industrial Informatics, vol.15, no.12, pp.6510–6521, 2019.

Yun Liang received his M.E. degree from Zhengzhou University. He is working in State Grid Henan Electric Power Grid Electric Power Scientific Research Institute. His main research interests are the application of IoT technology in power equipment monitoring, the research and application of key technology of power meteorology based on refined meteorological forecasting.

Degui Yao received his Ph.D degree from Chongqing University, China, in 2001. He is currently a Professor-Level Senior Engineer with the Electric Power Research Institute, State Grid Henan Electric Power Company. His research interest includes automation of electric power systems and core equipment operation and maintenance of UHV DC transmission technology and key technology research.
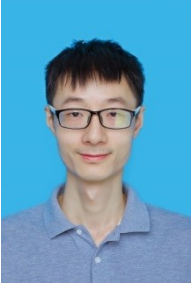
Yang Gao received his M.E. degree from Henan University. He is working in State Grid Henan Electric Power Grid Electric Power Scientific Research Institute. His research interests include power big data analysis and electric IoT. He mainly engaged in transmission line refined meteorological early warning technology and application, transmission line anti-dance spacer bar development and application research based on dynamic load bearing characteristics.

Kaihua Jiang received his Ph.D degree from Chongqing University, Chongqing, China in 2020. From September 2020 to November 2022, he was an engineer at the State Grid Zhejiang Electric Power Research Institute, China. Since December 2022, he has been a senior engineer at the same company. His research interests mainly focus on disaster prevention and mitigation technology of power system, on-line monitoring and fault diagnosis of electrical equipment.